Organic & Biomolecular Chemistry

Accepted Manuscript

This article can be cited before page numbers have been issued, to do this please use: Q. Peng, Y. Yuan, H. Zhang, S. Bo, Y. Li, S. Chen, Z. Yang, X. Zhou and Z. Jiang, *Org. Biomol. Chem.*, 2017, DOI: 10.1039/C7OB01068K.

ROYAL SOCIETY OF CHEMISTRY

rsc.li/obc

View Article Online
DOI: 10.1039/C7OB01068K

Organic & Biomolecular Chemistry

PAPER

^{19}F CEST imaging probes for metal ions detection

Qiaoli Peng,[a] Yaping Yuan,[b] Huaibin Zhang,[a] Shaowei Bo,[a] Yu Li,[a] Shizhen Chen,[b] Zhigang Yang,[a] Xin Zhou,[b] and Zhong-Xing Jiang*[abc]

Received 00th January 20xx,
Accepted 00th January 20xx

DOI: 10.1039/x0xx00000x

www.rsc.org/

To detecting metal ions with ^{19}F chemical exchange saturation transfer magnetic resonance imaging (^{19}F CEST MRI), a class of novel fluorinated chelators with diverse fluorine contents and chelation properties were conveniently synthesized on gram scales. From them, a DTPA derived chelator with high sensitivity and selectivity was identified as a novel ^{19}F CEST imaging probe for simutaneously detecting multiple metal ions.

Introduction

Metal ions are involved in numerous biological events and, therefore, monitoring the presence of certain metal ions and their local concentrations with novel imaging technology is of great importance for accurately understanding these biological events. Among the many imaging technologies,[1] ^{19}F MRI is very attractive because it provides quantitative images without ionizing radiation, tissue depth limit, and background signal.[2,3] To this end, some fluorinated chelators, such as *5,5'*-difluoro-*1,2*-bis(o-aminophenoxy) ethane-*N,N,N',N'*-tetraacetic acid (5F-BAPTA) and *5,5',6,6'*-tetrafluoro-*1,2*-bis(o-aminophenoxy) ethane-*N,N,N',N'*-tetraacetic acid (TF-BAPTA), were employed to monitor metal ions with either ^{19}F NMR by G. A. Smith et al[1c] and F. A. X. Schanne et al,[1d] or ^{19}F CEST by M. T. McMahon et al.[6] Although ^{19}F CEST MRI can dramatically amplify the signal of metal ion-bound fluorinated chelator, it is still very challenging to detect metal ions of low concentration with 5F-BAPTA or TF-BAPTA due to their limited ^{19}F MRI sensitivity. Without using high resolution ^{19}F MRI and extending the scan time, only a very weak ^{19}F signal can be generated from the two fluorine atoms in 5F-BAPTA and TF-BAPTA. In addition, it is very tedious to prepare these fluorinated chelators, especially on gram scales. Therefore, it is of great importance to develop novel easily available ^{19}F CEST imaging probes with high sensitivity and selectivity for monitoring metal ions at low concentration.

Herein, a class of fluorinated chelators **1-4** with multiple symmetric fluorines, single ^{19}F NMR peak, and controllable chelation property were designed as novel ^{19}F CEST imaging probes (Fig. 1). Multiple symmetrical fluorines, which collectively give a single ^{19}F NMR peak, were employed as a strong ^{19}F NMR/MRI

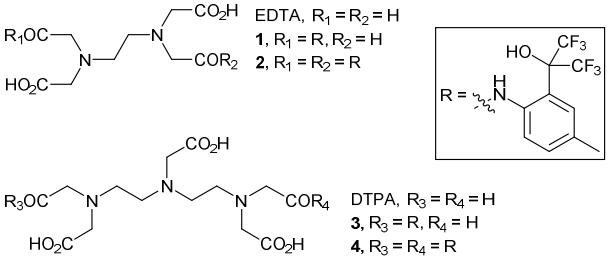

Figure 1. Structures of fluorinated chelators **1-4**.

aminetetraacetic acid (EDTA) and diethylenetriaminepentaacetic acid (DTPA) were selected as the backbones for chelators **1-4** due to their low price, easy availability, and high chelation selectivity on metal ions.[4] In order to achieve metal ion selectivity in ^{19}F CEST MRI, the number of the chelating groups in chelators **1-4** were tuned by the monoamide and diamide-derivatization of EDTA and DTPA, respectively. Besides the carboxylic groups in chelators **1-4**, the hydroxyl and amide groups are also available for metal ion chelation.[5] Because of the strong electron-withdraw effect of two adjacent trifluoromethyl groups, the hydroxyl groups in chelators **1-4** are actually very acidic which are good chelation groups for metal ion chelation.[5c,d] Once the hydroxyl and amide groups in chelators **1-4** chelated with metal ions, the electron environment of the fluorines changes accordingly which induces a ^{19}F NMR response, e.g., chemical shift change ($\Delta\omega$) and line broadening. If the exchange rate between metal ion-bound chelator and free chelator is slow enough ($k_{ex} < \Delta\omega$), a new peak will show up on the ^{19}F NMR spectra of chelators **1-4**. According to the mechanism of ^{19}F ion-CEST MRI,[6] i.e., using a radiofrequency to saturate the new peak from metal ion-bound chelator and detecting the saturation transfer to the free chelators, the signal of bound metal ions can be dramatically amplified.

Results and discussion

A convenient and scalable synthesis of fluorinated chelators **1-4** was developed, in which the amidation reaction between dianhydrides **5**, **6** and fluorinated aniline **7**, respectively, was employed as the key step (Scheme 1). Fresh dianhydrides **5** and **6**, which are also commercially available, were prepared by dehydration of EDTA and DTPA with acetic anhydride in the

[a] *Hubei Province Engineering and Technology Research Center for Fluorinated Pharmaceuticals and School of Pharmaceutical Sciences, Wuhan University, Wuhan 430071, China.*
[b] *State Key Laboratory for Magnetic Resonance and Atomic and Molecular Physics, Wuhan Institute of Physics and Mathematics, Chinese Academy of Sciences, Wuhan 430071, China.*
[c] *State Key Laboratory for Modification of Chemical Fibers and Polymer Materials, Dong Hua University, Shanghai 201620, China.*
† Emails of corresponding authors: zgyang@whu.edu.cn; zxjiang@whu.edu.cn.

Electronic Supplementary Information (ESI) available: ^{19}F NMR of chelators in the presence of Cu^{2+}, Fe^{3+}, EDTA and DTPA, association constant of chelators with metal ions, copies of ^{1}H/^{13}C NMR, MS/HRMS spectra, HPLC chromatograms. See DOI: 10.1039/x0xx00000x

View Article Online
DOI: 10.1039/C7OB01068K

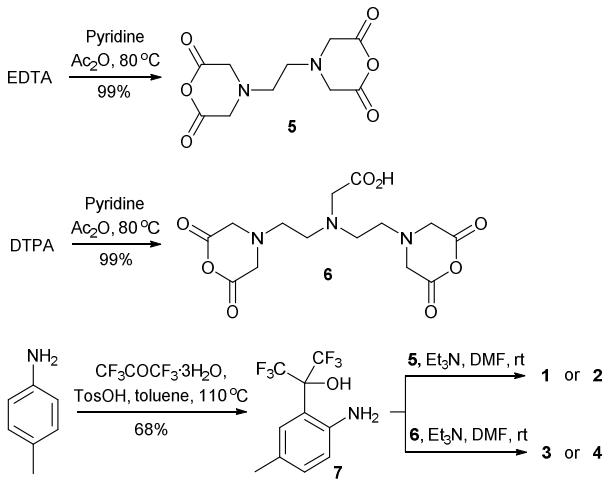

Scheme 1. Synthesis of fluorinated chelators **1-4**

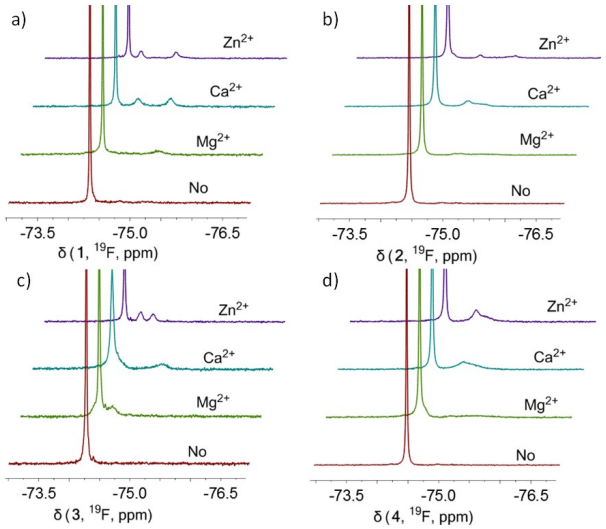

Figure 2. ^{19}F NMR of free chelators and Mg^{2+}, Ca^{2+}, Zn^{2+}-bound chelators **1** (a), **2** (b), **3** (c), and **4** (d). Each sample contained 0.8 mM metal ions and 4.0 mM chelators in 40 mM Hepes buffer at pH 7.2.

presence of pyridine, respectively.[7] Fluorinated amine **7** with a bis(trifluoromethyl)-carbinol moiety was then prepared through a Friedel-Crafts reaction of hexafluoroacetone trihydrate on 4-methylaniline in the presence of *p*-toluenesulfonic acid.[8] Monoazides **1**, **3** and diamides **2**, **4** were selectively prepared by tuning the relative amount of amine **7** and dianhydride **5**, **6** during the amidation reaction, respectively. It is noteworthy that the hydroxyl group in **7** is very inert during the amidation reactions because the two adjacent trifluoromethyl groups dramatically lowered the reactivity by increasing its acidity and steric hindrance. To guarantee high purity of the fluorinated chelators **1-4**, the amidation reaction mixtures were purified with preparative HPLC. Finally, fluorinated chelators **1-4** were prepared on 0.61-2.25 gram scales with good yields and high purities, respectively.

As poor water solubility of fluorinated compounds always limited their application in biological systems, the water solubility of chelators **1-4** was then investigated. It was found that the water solubility of chelators **1-4** is closely related to their fluorine contents (F%). Low F% chelators **1** (21%) and **3** (18%) are soluble in water at a wide pH range of 0 to 14 while high F% chelators **2** (28%) and **4** (25%) are soluble in water only at pH above 6 and 5, respectively. Therefore, all the fluorinated chelators **1-4** have no solubility issue for downstream ^{19}F NMR/MRI study around physiological pH.

As expected, each chelator produces a single ^{19}F NMR peak from multiple symmetrical fluorines which is ideal for detecting the chelator at low concentration (red peaks in Fig. 1). To study the chelation effects on ^{19}F NMR, ^{19}F NMR spectra of chelators **1-4** in the presence of Mg^{2+}, Ca^{2+}, Fe^{3+}, Cu^{2+}, and Zn^{2+} were collected. After chelating with Fe^{3+} and Cu^{2+}, no observable new ^{19}F NMR peaks can be detected on the ^{19}F NMR spectra of chelators **1-4** (Fig. S1 in ESI†). In contrast, well-defined new ^{19}F NMR peaks on ^{19}F NMR spectra of chelators 1-4 were detected in the presence of Mg^{2+}, Ca^{2+} and Zn^{2+} (Fig. 2). For chelators **1-3**, multiple chelation peaks were detected in the presence of Ca^{2+} and Zn^{2+} which is correspond to multiple species formed between the chelator and metal ion.[9] It is very important to point out that each free chelator **1-4** produces a singlet ^{19}F NMR peak around -74.4 ppm, respectively, with a small $\Delta\omega$ of 0.2 ppm despite their structural difference. Even after chelation with metal ions, the $\Delta\omega$ between free chelators and metal ion bound-chelators is less than 1 ppm. The small $\Delta\omega$ values indicate that metal ion chelation has limited influence on the electron environment of the fluorines because multiple C-C single bonds significantly blocked the chelation effect. As a comparison, $\Delta\omega$ of free TF-BAPTA and Zn^{2+}-bound TF-BAPTA reaches 10.5 ppm because the aromatic system can efficiently transfer the chelation effect to fluorines.[6] The appearance of well-defined new ^{19}F NMR peaks also indicates that the exchange between metal ion-bound chelator and free chelator is very slow ($k_{ex} < \Delta\omega$), which is fit for generating ^{19}F CEST contrast. Chelator **4** was chosen for downstream ^{19}F CEST study for two reasons. On one hand, chelator **4** has a singlet ^{19}F NMR peak from twelve fluorines which can dramatically improve the ^{19}F MRI sensitivity and lower the detectable concentration. On the other hand, a single ^{19}F NMR peak from free and metal ion-bound chelator **4**, respectively, can simplify the ^{19}F CEST process by avoiding the suppression of nearby peaks (Fig. 2d).

The influence factors, including metal ion concentration, pH, temperature, and addition of fast exchange metal ions, on the ^{19}F NMR of free and ions-bound chelator **4** were also studied. The Ca^{2+} concentration-dependent ^{19}F NMR showed that chelator **4** and Ca^{2+} formed a complex with a broad ^{19}F NMR peak around -74.9 ppm. A well-defined peak can be observed when the Ca^{2+}/chelator ratio is larger than 1/10 (Fig. 3a). The pH-dependent ^{19}F NMR showed that pH 6.0-7.5, which is within physiological pH, is the best range for detecting the Ca^{2+}-bound chelator **4** with ^{19}F NMR (Fig. 3b). It is noteworthy that very little chemical shift change was found in the range of pH 6.0-7.5, i.e. $\Delta\omega$= 0.07 for Ca^{2+}-bound and free chelator **4**, respectively. The addition of fast exchanging ions K^+ resulted in no observable ^{19}F NMR line broadening or chemical shift change, while the addition of Mg^{2+} resulted in observable ^{19}F NMR line broadening of free chelator **4** peak (Fig. 3c). Temperature-dependent ^{19}F NMR showed no line broaden for free chelator **4** and, while, obvious line sharpens for Ca^{2+}-chelator **4** at elevated temperature (Fig. 3d).[10] It was also found that, in the range of 283 K to 310 K,

View Article Online
DOI: 10.1039/C7OB01068K

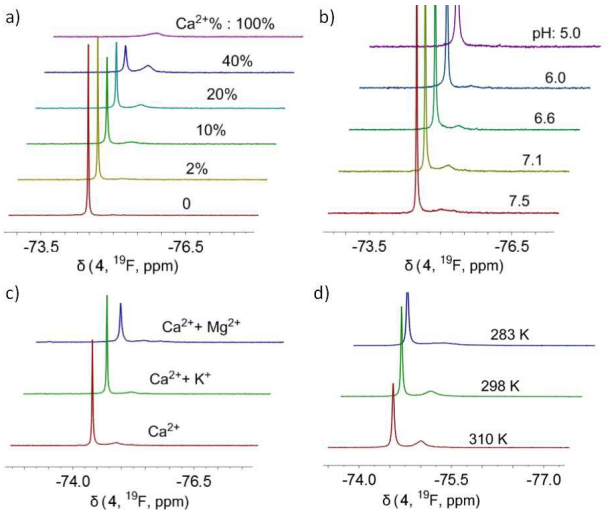

Figure 3. Concentration (a, Ca^{2+}% = [Ca^{2+}]/[chelator **4**] × 100%), pH (b), additive (c, 100 mM K^+ and 0.8 mM Mg^{2+}), and temperature-dependent (d) ^{19}F NMR of chelators **4**. Each sample contained 4.0 mM chelators **4** and 0.4 mM Ca^{2+}(b, c) or 0.8 mM Ca^{2+}(d) in 40 mM Hepes buffer at pH 7.2.

observable chemical shift change (Δω = 0.2 ppm) was observed for both free and Ca^{2+}-bound chelator **4**. In contrast to 5F-BAPTA of which the ^{19}F NMR chemical shift is very sensitive to pH, temperature, and fast exchanging ions, chelator **4** shows little response to these influence factors but to temperature. Therefore, using chelator **4** in ^{19}F NMR and ^{19}F MRI can actually avoid the image artifact and chemical shift calibration, which dramatically simplifies the ^{19}F NMR and ^{19}F CEST MRI process.

To evaluate the ^{19}F metal ion induced CEST (iCEST) effect of metal ions, the pH and metal ion-dependent Z-spectra of chelator **4** were collected. On one hand, an iCEST effect for Ca^{2+} at Δω = 0.4 ppm was observed from the pH-dependent Z-spectra (Fig. 4a-d). Because Ca^{2+}-bound chelator **4** dissociates under weak acidic conditions, a pronounced iCEST effect can only be found when pH > 6.0. On the other hand, an iCEST effect can be found for other selected metal ions. For Mg^{2+}, a well-defined iCEST effect on chelator **4** at Δω = 0.6 ppm was found (Fig. 4f), while an iCEST effect was found at Δω = 0.4 ppm for Zn^{2+} (Fig. 4h). Thus, by tuning the frequency of saturation pulse, it is feasible for chelator **4** to selectively detecting Mg^{2+}, Ca^{2+}, and Zn^{2+} using ^{19}F CEST MRI.

^{19}F iCEST MRI on metal ions was carried out on a 9.4 T scanner. Firstly, selective ^{19}F iCEST MRI of chelator **4** on Mg^{2+}, Ca^{2+}, and Zn^{2+} was studied (Fig. 5). ^{19}F MRI of four tubes containing 5 mM chelator **4** and 50 μM each metal ions showed no noticeable contrast (Fig. 5a). However, when a saturation pulse was applied at Δω = 0.4 ppm, ^{19}F iCEST images showed clear contrast for the tubes containing Ca^{2+} and Zn^{2+} with contrast percentile of 20% and 19%, respectively (Fig. 5b). When a saturation pulse was applied at Δω = 0.6 ppm, only the tube containing Mg^{2+} showed clear contrast ^{19}F iCEST images with contrast percentile of 17% (Fig. 5c). Therefore, using chelator **4**, it is feasible to selectively detect Mg^{2+} at Δω = 0.6 ppm and simultaneously detect both Ca^{2+} and Zn^{2+} at Δω = 0.4 ppm using ^{19}F iCEST MRI. Although the Δω is pretty small, the chemical shift insensitive nature of free and metal ion bound-chelator **4** to pH, temperature, and fast exchanging ions makes the ^{19}F iCEST MRI process straightforward. Secondly, the selective ^{19}F iCEST MRI of Mg^{2+} in the presence of Ca^{2+}, Zn^{2+} and vice versa were studied.

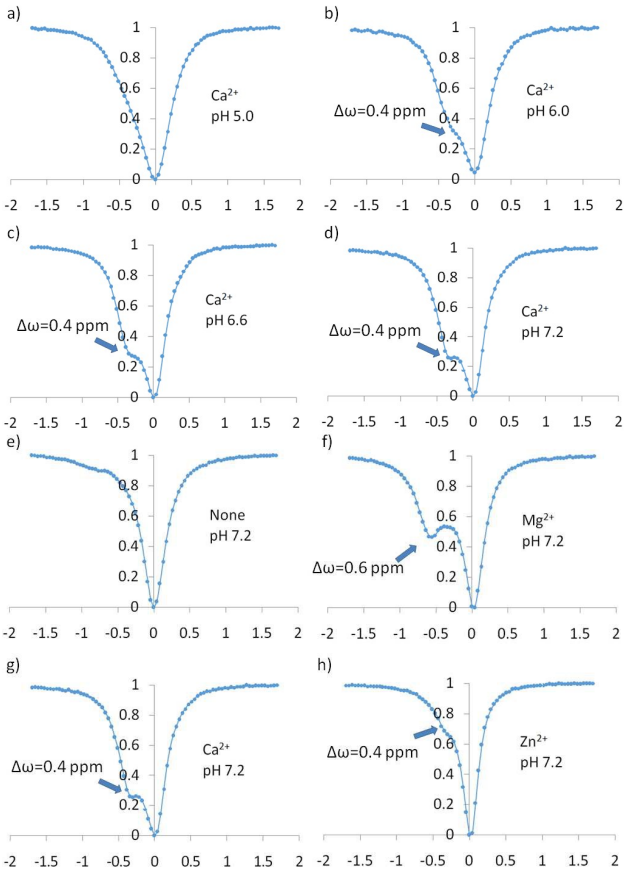

Figure 4. pH (a-d) and metal ion-dependent (e, none; f, Mg^{2+}; g, Ca^{2+}; h, Zn^{2+}) Z-spectra of chelator **4** and Ca^{2+}. Each sample contained 2.0 mM chelator **4** and 0.2 mM Ca^{2+} in 40 mM Hepes buffer at the indicated pH.

Clear contrast for Mg^{2+} at Δω = 0.6 ppm can still be observed in the presence of coexisting ions Ca^{2+} and Zn^{2+} (Fig. 5f). In the meanwhile, it can also selectively detect Ca^{2+} and Zn^{2+} in the metal ion-bound chelator **4** comparing to that of EDTA was evaluated with ^{19}F iCEST MRI. In the presence of 1 mM EDTA, competing chelating reactions for metal ions between EDTA and chelator **4** took place. It turned out that Mg^{2+}, Ca^{2+}, and Zn^{2+} form much more stable complex with EDTA than these of chelator **4** because no ^{19}F iCEST MRI was observed at either 0.4 ppm or 0.6 ppm. Association constant measurement of chelators **1**-**4** with Mg^{2+}, Ca^{2+}, and Zn^{2+} through a titration method[11] indicated that the EDTA and DTPA have higher binding affinities towards these metal ions than that of the corresponding fluorinated chelators (Fig. S3 and Table S1 in ESI†). Thus, addition of EDTA can turn off the ^{19}F iCEST MRI by preventing the formation of metal ion bound-chelator **4**. In this way, an on and off-^{19}F iCEST MRI strategy for selectively detecting metal ions can be developed. Because each metal ion has quite unique stability constant with commercially available chelators, such as EDTA, DTPA, DOTA, etc., it is possible to selectively turn off ^{19}F iCEST MRI by addition of a commercially available chelator to a metal ions mixture and selectively chelating the ^{19}F iCEST MRI-generating metal ion(s). Based on these observation, Mg^{2+}, Ca^{2+}, and Zn^{2+} can be sensitively and selectively detected with chelator **4** by ^{19}F iCEST MRI at a concentration as low as 50 μM.

To investigate the sensitivity of using chelator **4** in detecting Mg^{2+} with ^{19}F iCEST MRI, a Mg^{2+} concentration-dependent ^{19}F iCEST MRI was then carried out (Fig. 6). It was found that Mg^{2+} can

View Article Online
DOI: 10.1039/C7OB01068K

be detected at a concentration 10 μM. In this case, a magnetization transfer ratio (MTR) of 11% was observed at a Mg^{2+}/**4** ratio of 1:500 with a data collection time of 6.5 minutes.

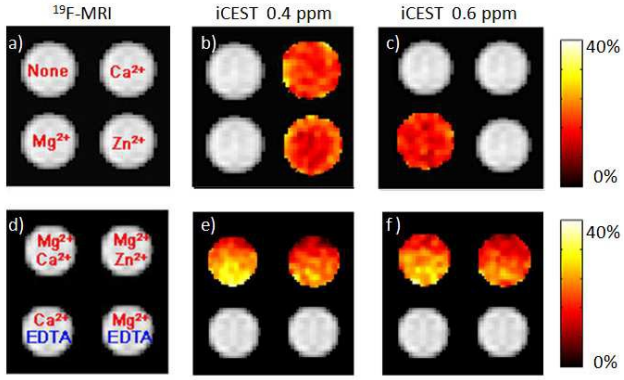

Figure 5. ^{19}F iCEST MRI of chelator **4** in the presence of metal ions Mg^{2+}, Ca^{2+}, Zn^{2+}, and EDTA. Each sample contained 5 mM chelator **4** and 50 μM indicated metal ion, respectively. Sample d-f were added extra 50 μM of Mg^{2+} or 1 mM EDTA, respectively.

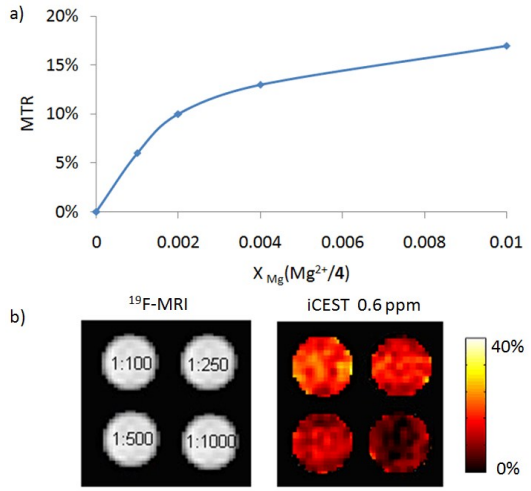

Figure 6. (a) Plot of magnetization transfer ratio (MTR) vs X_{Mg}. (b) ^{19}F iCEST MRI of chelator **4** in the presence of Mg^{2+}. Alignment of four tubes containing 5 mM of **4** and different concentrations of Mg^{2+} (X_{Mg} =1:100, 1:250, 1:500, 1:1000).

Conclusions and prospects

In this study, we have developed a class of novel ^{19}F CEST imaging probes and applied them in sensitively and selectively detecting metal ions with ^{19}F iCEST MRI. These imaging probes with a strong and singlet ^{19}F NMR peak from multiple fluorines can be conveniently prepared on gram scales from commercially available chelators. Comparing to known fluorinated metal ion chelators, ^{19}F NMR chemical shift of these chelators is not sensitive to environment, e.g. pH and temperature, but sensitive of certain metal ions, which turns these chelators into selective ^{19}F imaging probes for these metal ions. However, the chemical shift changes induced by the metal ions in quite low, < 1 ppm, comparing to 10.5 ppm from TF-BAPTA. By tuning the frequency of saturation pulse, multiple ions, especially for Mg^{2+}, can be selectively detected by ^{19}F iCEST MRI with one of these probes. Because of the symmetrical distribution of twelve fluorines, the probe exhibit enhanced sensitivity for detecting metal ions at low concentration. To imaging metal ions *in vivo* with ^{19}F iCEST MRI, some fine tunes on sensitivity, selectivity, chelation property, and physicochemical properties of the existing probes are always required. The study here has illustrated a fine tune strategy to enhance the sensitivity of the ^{19}F imaging probe while maintain its metal ion selectivity by constructing novel fluorinated chelators. Further fine tunes on the structure of the probes to improve the selectivity on multiple metal ions are actively going on in this group.

Experimental

General information

^{1}H, ^{19}F and ^{13}C NMR spectra of chelators were recorded on a 400 MHz. Chemical shifts are in ppm and coupling constants (*J*) are in Hertz (Hz). ^{1}H NMR spectra were referenced to solvent hydrogens (3.31 ppm) using CD_3OD as solvent. ^{13}C NMR spectra were referenced to solvent carbons (m, 49.64-48.36 ppm for CD_3OD). ^{19}F NMR spectra were referenced to 2% perfluorobenzene (s, -164.90 ppm) in CD_3OD or sodium trifluomethanesulfonate (s, -79.61 ppm) in D_2O. The splitting patterns for ^{1}H NMR spectra are denoted as follows: s (singlet), d (doublet), q (quartet), m (multiplet). Unless otherwise indicated, all reagents were obtained from commercial supplier and used without prior purification. DMF, Et_3N and Pyridine were dried and freshly distilled prior to use.

^{19}F MRI experiments were performed on a 9.4 T micro-imaging system with a 10 mm inner diameter ^{19}F coil (376.4 MHz) for both radiofrequency transmission and reception. The RARE sequence was employed for all MRI acquisitions with single average. RARE factor=4, TR=6000 ms, TE=5.37 ms, matrix=32*32, Number of average=4, FOV=30 mm*30 mm, slice thickness=20 mm, Saturation pulse strength =1 uT, Saturation time=3 s.

General procedure for the preparation of compounds 1-4

compound 5. A slurry of EDTA (2.92 g, 10.00 mmol), dry pyridine (4.75 g, 60.00 mmol), and acetic anhydride (4.08 g, 40.00 mmol) was heat to 80 °C and stirred at this temperature for 24 h. After cooled to room temperature, the reaction mixture was filtered. The solid residue was washed with acetic anhydride and diethyl ether to yield **5** as white solid (2.56 g, yield 99%). ^{1}H NMR (400 MHz, d-DMSO) δ 3.70 (s, 8H), 2.66 (s, 4H).

Compound 6. Diethylenetriaminepentaacetic acid bisanhydride **6** was prepared by following the same procedure for **5** as white solid (3.93 g, yield 99%). ^{1}H NMR (400 MHz, d-DMSO): δ 2.60 (t, *J* = 6.2 Hz, 4H), 2.76 (t, *J* = 6.2 Hz, 4H), 3.44 (s, 2H), 3.72 (s, 8H).

Compound 7. To a sealed vessel was added 4-methylaniline (4.00 g, 37.33 mmol), 4-toluene sulfonic acid monohydrate (0.71 g, 3.73 mmol), 1,1,1,3,3,3-hexafluoroacetone trihydrate (12.32 g, 55.99 mmol) and toluene (25 mL). The vessel was sealed up and stirred for 8 h at 110 °C. The solution was concentrated under vacuum and the residue was purified by flash chromatography on silica gel (petroleum ether/ethyl acetate = 9/1) to give compound **7** as white

View Article Online
DOI: 10.1039/C7OB01068K

needles (6.93 g, yield 68%). ^{1}H NMR (400 MHz, $CDCl_3$) δ 7.38 (s, 1H), 7.17 (d, *J* = 8.0 Hz, 1H), 6.97 (d, *J* = 8.0 Hz, 1H), 2.36 (s, 3H); ^{19}F NMR (376 MHz, $CDCl_3$) δ -78.41.

Compound 1. To a stirring solution of EDTA dianhydride **5** (1.02 g, 4.00 mmol) in DMF (35 mL) and triethylamine (1.62 g, 16.00 mmol) was added a solution of amine **7** (0.55 g, 2.00 mmol) in 8 mL DMF dropwise under an atmosphere of nitrogen at 0 °C. After the addition, the mixture was stirred at 0 °C for 1 h and room temperature for another 8 h. The reaction was quenched with H_2O and the solvent was evaporated under vacuum. The residue was purified with preparative RP-HPLC to give **1** (0.61 g, yield 56%) as white solid. ^{1}H NMR (400 MHz, CD_3OD) δ 8.07 (d, *J* = 8.2 Hz, 1H), 7.38 (s, 1H), 7.32 (d, *J* = 8.5 Hz, 1H), 4.11 (s, 4H), 3.96 (s, 2H), 3.90 (s, 2H), 3.44 (t, *J* = 5.4 Hz, 2H), 3.35 (t, *J* = 5.5 Hz, 2H), 2.35 (s, 3H); ^{13}C NMR (100 MHz, CD_3OD) δ 172.3, 170.9, 168.7, 136.2, 135.9, 132.2, 129.4, 126.8, 124.4 (q, *J* = 289.6 Hz), 120.1, 82.0-80.9 (m), 58.5, 55.8, 53.5, 52.2, 21.0; ^{19}F NMR (376 MHz, CD_3OD) δ -74.69; HRMS (ESI) calcd for $C_{20}H_{22}F_6N_3O_8^-$ ([M-H]$^-$), 546.1317, found, 546.1328.

Compound 2. Chelator **2** was prepared by following the same procedure for chelator **1** as white solid (1.30 g, yield 81%). ^{1}H NMR (400 MHz, CD_3OD) δ 8.08 (d, *J* = 8.1 Hz, 2H), 7.36 (s, 2H), 7.22 (d, *J* = 8.1 Hz, 2H), 3.84 (s, 4H), 3.80 (s, 4H), 3.25 (s, 4H), 2.33 (s, 6H). ^{13}C NMR (100 MHz, CD_3OD) δ 171.6, 167.7, 136.0, 132.1, 129.4, 126.9, 124.3 (q, *J* = 288.4 Hz), 121.2, 82.0-80.8(m), 58.4, 55.9, 53.1, 21.1; ^{19}F NMR (376 MHz, CD_3OD) δ -74.69; HRMS (ESI) calcd for $C_{30}H_{29}F_{12}N_4O_8^-$ ([M-H]$^-$), 801.1799, found, 801.1798.

Compound 3. To a stirring solution of DTPA dianhydride **6** (1.43 g, 4.00 mmol) and triethylamine (1.62 g, 16.00 mmol) in DMF (35 mL) was dropwise added amine **7** (0.55 g, 2.00 mmol) in DMF (8 mL) under an atmosphere of nitrogen at 0 °C and the mixture was stirred at this temperature for 1 h. After warm to room temperature, the mixture was stirred at room temperature for additional 8 h. The reaction was quenched with H_2O and the solvent was evaporated under vacuum. The residue was purified with preparative RP-HPLC to give **3** (0.79 g, yield 61%) as white solid. ^{1}H NMR (400 MHz, CD_3OD) δ 8.14 (d, *J* = 8.6 Hz, 1H), 7.38 (s, 1H), 7.33 (d, *J* = 8.5 Hz, 1H), 4.17 (s, 2H), 3.85 (s, 2H), 3.80 (s, 6H), 3.52-3.35 (m, 8H), 2.35 (s, 3H); ^{13}C NMR (100 MHz, CD_3OD) δ 174.4, 173.7, 170.8, 169.4, 136.6, 135.4, 132.2, 129.4, 125.9, 123.0, 120.2, 82.0-80.9 (m), 59.0, 56.0, 54.9, 54.7, 54.3, 51.3, 50.9, 21.0; ^{19}F NMR (376 MHz, CD_3OD) δ -74.64; HRMS (ESI) calcd for $C_{24}H_{29}F_6N_4O_{10}^-$ ([M-H]$^-$), 647.1793, found, 647.1796.

Compound 4. Chelator **4** was prepared by following the same procedure for chelator **3** as white solid (2.25 g, yield 83%). ^{1}H NMR (400 MHz, CD_3OD) δ 8.09 (d, *J* = 8.3 Hz, 2H), 7.35 (s, 2H), 7.26 (d, *J* = 8.5 Hz, 2H), 4.19 (s, 2H), 3.78 (s, 4H), 3.73 (s, 4H), 3.48 (t, *J* = 6.1 Hz, 4H), 3.33(t, *J* = 6.2 Hz, 4H), 2.33 (s, 6H); ^{13}C NMR (100 MHz, CD_3OD) δ 173.1, 169.9, 169.8, 136.3, 135.6, 132.2, 129.3, 126.3, 124.4 (q, *J* = 288.7 Hz), 120.6, 82.1-80.9 (m), 58.9, 56.0, 54.8, 54.1, 51.6, 21.0; ^{19}F NMR (376 MHz, CD_3OD) δ -74.69; HRMS (ESI) calcd for $C_{34}H_{36}F_{12}N_5O_{10}^-$ ([M-H]$^-$), 902.2276, found, 902.2259.

Acknowledgements

We are thankful for financial support from the National Key Research and Development Program of China (2016YFC1304704), the National Natural Science Foundation of China (21372181, 21402144 and 21572168), and State Key Laboratory for Magnetic Resonance and Atomic and Molecular Physics (Wuhan Institute of Physics and Mathematics).

Notes and references

1 (a) K. P. Carter, A. M. Young, A. E. Palmer, *Chem. Rev.*, 2014, **114**, 4564-4601; (b) R. Y. Tsien, *Biochemistry*, 1980, **19**, 2396-2404; (c) G. A. Smith, R. T. Hesketh, J. C. Metcalfe, J. Feeney, P. G. Morris, *Proc. Natl. Acad. Sci. USA*, 1983, **80**, 7178-7182; (d) F. A. X. Schanne, T. L. Dowd, R. K. Gupta, J. F. Rosen, *Proc. Natl. Acad. Sci. USA*, 1989, **86**, 5133-5135; (e) H. Komatsu, T. Miki, D. Citterio, T. Kuboba, Y. Shindo, Y. Kitamura, K. Oka, K. Suzuki, *J. Am. Chem. Soc.*, 2005, **127**, 10798-10799; (f) T. Nishihara, Y. Kameyama, H. Nonaka, Y. Takakusagi, F. Hyodo, K. Ichikawa, S. Sando, *Chem. Asian J.*, 2017, **12,** 949-953.

2. (a) E. T. Ahrens, R. Flores, H. Xu, P. A. Morel, *Nat. Biotechnol.*, 2005, **23**, 983-987; (b) J. M. Janjic, M. Srinivas, D. K. Kadayakkara, E. T. Ahrens, *J. Am. Chem. Soc.*, 2008, **130**, 2832-2841; (c) Z.-X. Jiang, X. Liu, E. K. Jeong, Y. B. Yu, *Angew. Chem., Int. Ed.*, 2009, **48**, 4755-4758; (d) J. Ruiz-Cabell, B. P. Barnett, P. A. Bottomley, J. W. M. Bulte, *NMR Biomed.*, 2011, **24**, 114-129; (e) D. Vivian, K. Cheng, S. Khuranan, S. Xu, E. H. Kriel, P. A. Dawson, J. P. Raufman, J. E. Polli, *Mol. Pharm.*, 2014, **11**, 1575-1582; (f) S. Langereis, J. Keupp, J. L. J. van Velthoven, I. H. C. de Roos, D. Burdinski, J. A. Pikkemaat, H. Grüll, *J. Am. Chem. Soc.*, 2009, **131**, 1380-1381.

3. (a) C. Zhang, S. S. Moonshi, H. Peng, S. Puttick, J. Reid, S. Bernardi, D. J. Searles, A. K. Whittaker, *ACS Sens*., 2016, **1**, 757-765; (b) D. Xie, S. Kim, V. Kohli, A. Banerjee, M. Yu, J. S. Enriquez, J. J. Luci, E. L. Que, *Inorg. Chem.*, 2017, **56**, 6429-6437; (c)T. Nakamura, H. Matsushita, F.Sugihara, Y. Yoshioka, S. Mizukami, K. Kikuchi, *Angew. Chem.*, *Int. Ed.,* 2015, **54**, 1007–1010.

4. (a) R. Hagen, J. P. Warren, D. H. Hunter, J. D. Roberts, *J. Am. Chem. Soc.*, 1973, **95**, 5712-5716; (b) N. Illy, D. Majonis, I. Herrera, O. Ornatsky, M. A. Winnik, *Biomacromolecules*, 2012, **13**, 2359-2369; (c) J. S. Summers, J. B. Baker, D. Meyerstein, A. Mizrahi, I. Zilbermann, H. Cohen, C. M. Wilson, J. R. Jones, *J. Am. Chem. Soc.*, 2008, **130,** 1727-1734.

5. (a) G. E. Fryxell, W. Chouyyok, R. D. Rutledge, *Inorg. Chem. Commun.*, 2011, **14** , 971-974; (b) J. C. Joyner, L. Hocharoen, J. A. Cowan, *J. Am. Chem. Soc.*, 2012, **134**, 3396-3410; (c) L. Tahsini, S. E. Specht, J. S. Lum, J. J. M. Nelson, A. F. Long, J. A. Golen, A. L. Rheingold, L. H. Doerrer, *Inorg. Chem.*, 2013, **52**, 14050–14063; (d) S. A. Cantalupo, S. R. Fiedler, M. P. Shores, A. L. Rheingold, L. H. Doerrer, *Angew. Chem. Int. Ed.*, 2012, **51**, 1000–1005.

6. (a) A. Bar-Shir, A. A. Gilad, K. W. Y. Chan, G. Liu, P. C. M. van Zijl, J. W. M. Bulte, M. T. McMahon, *J. Am. Chem. Soc.*,

View Article Online
DOI: 10.1039/C7OB01068K

2013, **135**, 12164-12167; (b) A. Bar-Shir, N. N. Yadav, A. A. Gilad, P. C. M. van Zijl, M. T. McMahon, J. W. M. Bulte, *J. Am. Chem. Soc.*, 2015, **137**, 78-81.

7. S. S. Kelkar, L. Xue, S. R. Turner, T. M. Reineke, *Biomacromolecules*, 2014, **15**, 1612-1624.
8. (a) W. Yu, Y. Yang, S. Bo, Y. Li, S. Chen, Z. Yang, X. Zheng, Z.-X. Jiang, X. Zhou, *J. Org. Chem.*, 2015, **80**, 4443-4449; (b) S. Bo, C. Song, Y. Li, W. Yu, S. Chen, X. Zhou, Z. Yang, X. Zheng, Z.-X. Jiang, *J. Org. Chem.*, 2015, **80**, 6360-6366; (c) Y. Li, G. Xia, Q. Guo, L. Wu, S. Chen, Z. Yang, W. Wang, Z.-Y. Zhang, X. Zhou, Z.-X. Jiang, *MedChemComm*, 2016, **7**, 1672-1680.
9. (a) M. Peana, S. Medici, V. M. Nurchi, J. I. Lachowicz, G. Crisponi, M. Crespo-Alonso, M. A. Santos, M. A. Zoroddu, *J. Inorg. Biochem.*, 2014, **141**, 132–143; (b) D. A. Dickie, R. A. Kemp, *Organometallics,* 2014, **33**, 6511−6518.
10. R. F. Evilia, *Inorg. Chem.*, 1985, **24**, 2076-2080.
11. (a) J. Bjerrum, "Metal Ammine Formation in Aqueous Solution," *P. Haase and Son, Copenhagen,* 1941; (b) M. Calvin, K. W. Wilson, *J. Am. Chem. Soc.*, 1945, **67**, 2003–2007; (c) S. Chaberek Jr., A. E. Martell, *J. Am. Chem. Soc.*, 1952, **74**, 5052–5056; (d) N. Türkel, *J. Chem. Eng. Data*, 2011, **56**, 2337–2342.

View Article Online
DOI: 10.1039/C7OB01068K

^{19}F CEST imaging probes for metal ions detection

Qiaoli Peng,[a] Yaping Yuan,[b] Huaibin Zhang,[a] Shaowei Bo,[a] Yu Li,[a] Shizhen Chen,[b] Zhigang Yang,[a] Xin Zhou,[b] and Zhong-Xing Jiang*[,a,b]

Graphical Abstract

An easily available fluorinated chelator was developed as a highly sensitive ^{19}F iCEST MRI probe for selectively detecting of metal ions.